Structure from Motion for the Creation of Realistic 3D Models of ISO Fine Test Dust

A THESIS SUBMITTED TO THE FACULTY OF THE GRADUATE SCHOOL OF THE UNIVERSITY OF MINNESOTA BY

Jared Ryan Moody

IN PARTIAL FULFILLMENT OF THE REQUIREMENTS FOR THE DEGREE OF PROFESSIONAL MASTER OF ENGINEERING

Professor Christopher J. Hogan Jr., Adviser

Professor Christopher J. Ellison, Co-Adviser

October 2021

ACKNOWLEDGEMENTS

I would like to thank my co-advisers, Professors Chris Hogan and Christopher Ellison. Professor Ellison provided invaluable help in identifying experts with relevant experience in the niche focus area of my project. Professor Hogan has been incredibly generous with his time and provided insightful advice again and again. He has fostered a research group that is truly special. I also wish to thank Devin McGee, who helped by printing hundreds of model dust particles and provided recommendations on the design of the packed bed.

I gratefully acknowledge my Donaldson colleague, Chad Goltzman, who presciently recommended an investigation into Structure from Motion.

Lastly, thank you to my family for their boundless support. My wife, Andi, showed me the patience of a saint. My oldest son, Oliver, served as an ambivalent lab assistant helping to time the packed bed trials. He summed up the experience thusly: “This is so boring.”

ABSTRACT

ISO Fine Arizona test dust is a typical surrogate contaminant for air filtration. Donaldson differential pressure simulations model dust particles as spheres. Filter performance is defined by terminal differential pressure and the rate at which it is achieved. Use of more realistic geometries is expected to improve simulation predictivity. Common characterization methods are insufficient to describe particle morphology in three dimensions. The present work lays out an accessible workflow using Structure from Motion, a photogrammetric technique, to convert a series of overlapping two-dimensional SEM micrographs into a three-dimensional dust model. The 3D workflow is informed by an analysis of 2D shape performed on thousands of ISO Fine particles. Packed bed experiments comparing realistic 3D-printed dust particles and volume-equivalent spheres demonstrate differentiated performance at a scale that is relevant to the filtration industry.

TABLE OF CONTENTS

LIST OF TABLES

LIST OF FIGURES

CHAPTER 1: BACKGROUND

Arizona test dust has been used as a surrogate contaminant for air filtration since at least 1940.[1] It remains one of the most commonly used contaminants in the filtration industry. To ensure uniformity of test dust over time: chemical composition, bulk density, and particle size distribution limits are specified.[2] However, other relevant properties such as dust shape are not tracked. Shape determines maximum packing density, which affects filter-level performance.[3] A filter with a denser dust cake will experience a higher differential pressure and poorer pulsability than an equivalently loaded filter with lower dust cake density.[4] It is therefore essential to understand dust morphology before one can predict filter performance.

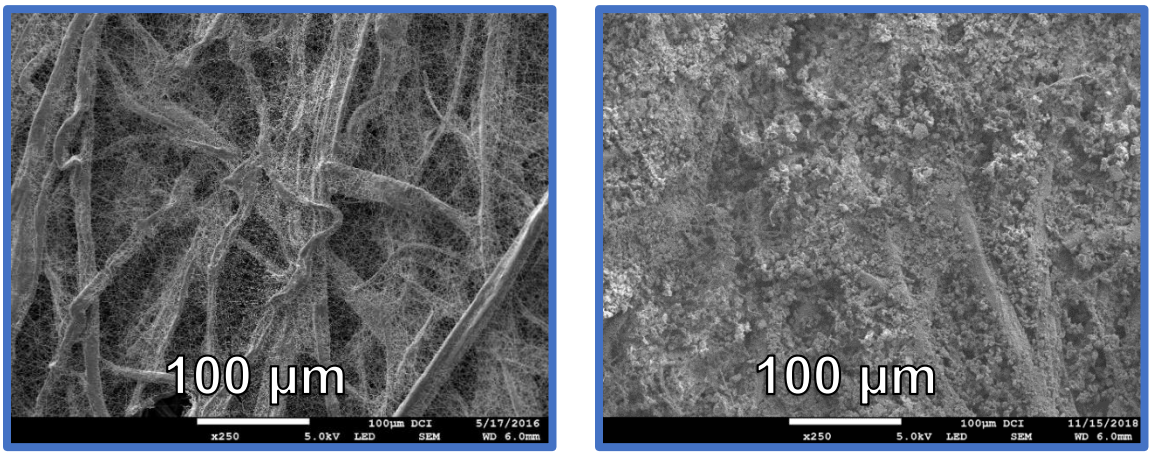

FIGURE 1. Clean Filter Media (left), Dust-Laden Filter Media (right)

Current Donaldson models and simulations treat challenge dusts as a collection of spheres. However, electron micrographs of Arizona test dust suggest this assumption is poor.[3] Nonthermally generated dust is rarely spherical. Figure 1 depicts a comparison of typical

clean and dust-laden filter media. The dust particles appear nonspherical and crystalline. It is desirable to incorporate more realistic dust morphologies into Donaldson models in order to accurately predict filter performance, specifically the pressure drop across a filter loaded with dust, as for the majority of their lifetimes, loaded dust is the largest contributor to pressure drop. The challenge is that dust particles are small and difficult to image in three dimensions. Most common approaches to characterize dust fall short of fully describing the morphology.

Laser diffraction particle size analyzers, like the Beckman Coulter LS 13 320, are commonly used to determine the particle size distribution of test dusts. However, they detect non-spherical particles in multiple orientations. Those orientations result in different diffraction patterns that are observed in aggregate. While limited deconvolution of aggregate diffraction patterns and estimation of shape properties is possible, in a Catch-22, detailed shape data is not accessible without *a priori* knowledge of shape.[5] Further, the wavelength of laser light places a lower limit on the size of detectable particles.

Scanning electron microscopy (SEM) can provide detailed shape analysis, but is typically limited to two dimensions. The International Organization for Standardization (ISO) highlights that while SEM can be utilized for assessing particle size and shape distribution, it only captures a two-dimensional projection for a specific viewing angle of the true three-dimensional shape.[6] It fails to accurately represent three-dimensional shape characteristics like height and texture. Previously, the National Institute of Standards and Technology (NIST) calculated the two-dimensional shape parameters of aspect ratio, longest chord to

projected area diameter ratio, and circularity of ISO Medium particles from SEM image boundaries.[7] NIST found shape and size to be only weakly correlated. The small subset of shape parameters calculated omits important factors like convexity and compactness. An analysis of two-dimensional ISO Fine shape parameters is included in this report as a first approach to characterize Arizona test dust morphology. Because this analysis is easier to perform on a statistically meaningful number of particles than the three-dimensional method proposed, it is used to inform the 3D analysis. Specifically, the correlation between ISO Fine size and shape parameters is probed to determine whether particles from all portions of the size range need to be measured in three dimensions in order to create a representative subset of 3D morphologies. Micro-computed tomography is regularly used to provide three-dimensional data. However, industrially available instruments typically lack submicron resolution.[8] Dust particle sizes relevant to modern air filtration are therefore inaccessible. Atomic force microscopy has the requisite spatial and dimensional resolution, but it is time consuming and practically challenging.[9] It is difficult to mount the particles with sufficient separation such that only one particle is probed at a time. Further, as a contact method, the AFM tip can easily dislodge or move particles of interest yielding incomplete or misleading shape data.

Given the importance of quantifying dust 3D structure for predicting pressure drop in dust-loaded filters, and the limitations of prior approaches in quantifying 3D dust structure, in this report, Structure from Motion (SfM) is used to translate a collection of 2D SEM micrographs into 3D models of individual ISO Fine dust particles.[10] SfM is a photogrammetric technique for reproducing a three-dimensional structure from a series of

overlapping two-dimensional images taken at different angles.[11] The movement of matching features is tracked from image to image and used to estimate the position of the features in space. The location of each feature can be plotted as a point, and the collection of points forms a point cloud. The points in the point cloud are connected with their nearest neighbors to form a mesh, which approximates the three-dimensional object.

SfM is commonly used with real cameras in fields like archaeology.[12, 13] In a typical scheme, the camera is moved around a fixed object. The application of SfM to SEM presents some challenges. Instead of a fixed object and mobile camera, an SEM has a fixed detector and mobile object. More importantly, most software built to perform SfM analysis assumes the images are collected with a standard camera that detects light. They are not built for SEM images that, while analogous, are not the same.

Overall, this analysis is broken into three phases. In phase one, two-dimensional shape statistics are collected for ISO Fine test dust from SEM micrographs. In phase two, the 2D shape statistics are used to select dust particles for 3D SfM modeling that are representative of typical ISO Fine particles. Ideally, a large number of particles would be fully modeled in 3D. Unfortunately, the modeling process is time intensive. It requires about three hours of image collection, 30 minutes of SfM analysis, and 30 minutes of model clean up to produce a single high-fidelity model. Out of practicality, only a small number of particles are modeled in 3D. In phase three, the 3D models are printed in a variety of sizes (according to 2D particle size distribution data) and used to perform pressure drop experiments.

CHAPTER 2: TWO-DIMENSIONAL SHAPE ANALYSIS

Despite the ubiquitous use of Arizona test dust, relatively little has been published about its shape characteristics. This is surprising given that particle shape is expected to be a key input for predicting pressure drop across a loaded filter. This situation is commonly modeled as fluid differential pressure through a packed bed with the Kozeny-Carman equation (1):[14]

$$\frac{\Delta p}{L} = -\frac{150\mu}{\Phi_s^2 D_p^2}\frac{(1-\epsilon)^2}{\epsilon^3} v_s \qquad (1)$$

where Δp is pressure drop, L is packed bed length, μ is the dynamic viscosity of the fluid, v_s is superficial fluid velocity, ϵ is the void fraction of the packed bed, Φ_s is the sphericity of the packing particle, and D_p is the diameter of a volume-equivalent sphere for the packing particle. Kozeny-Carman predicts that pressure drop varies as the inverse of the square of particle sphericity. Sphericity is less than one for nonspherical particles, which is expected to lead to higher pressure drops due to frictional losses. However, void fraction is a complex function of particle shape and other factors. There are shapes for which void fraction can increase or decrease relative to their spherical equivalents.

In one of the few studies available, Fletcher and Bright visually analyzed a small number of shape factors (aspect ratio, circularity, and longest chord/project area diameter) of ISO Medium test dust from SEM micrographs.[7] ISO Medium is a related distribution of Arizona Test dust with a larger average particle diameter than the ISO Fine studied here.[2] Fletcher and Bright found that ISO Medium shape factors were not strongly dependent on particle

size. If this held true for ISO Fine, it would reduce the number of modeled particles required to accurately represent the overall distribution.

In this investigation, I applied a similar approach to ISO Fine using a much broader array of descriptive shape statistics. The main goal of this approach was to begin to understand the variability in the shape of ISO Fine dust particles in two dimensions and then use that information to inform any further three-dimensional consideration of shape. The following five-step process was used to collect 2D shape statistics:

1. Disperse particles in deionized water. Thin the dispersion through serial dilutions. Filter the dilute dispersion onto a membrane.
2. Sputter coat the membrane and image at multiple magnifications between 25x and 5000x with SEM.
3. Use Trainable Weka Segmentation in Fiji to create a probability map of particle locations on SEM images.[15] Binarize the probability map to create an image where black pixels represent particles and white pixels represent background.
4. Use Tunwal *et al.*'s Image based Particle Shape Analysis Toolbox (IPSAT) for Mathematica to calculate multiple shape and size parameters.[16]
5. Analyze particle statistics for trends with JMP.

In step one, 0.1 g of ISO Fine dust was added to 100 mL of deionized water. The mixture was mechanically agitated, but no chemical dispersants were added. The dispersion was then twice diluted in a 1:100 ratio in serial fashion. Finally, the dilute dispersion was

vacuum filtered onto a 0.22-micron membrane patch. Dispersion was necessary to reduce the number of particles touching and overlapping, which confounds automated image analysis. The amount of dust was selected such that if the particles were spherical, they would be expected to obscure approximately 10% of the area of the 47-mm diameter membrane patch.

In step two, samples were mounted and sputter coated with a gold/palladium target in preparation for SEM imaging. Samples were imaged with a Jeol JSM 7100 microscope (accelerating voltage: 25 kV, working distance: 5.9 mm) at 25x, 50x, 100x, 250x, 500x, 1000x, 2500x, and 5000x magnifications. Up to 20 images were collected. Only magnifications between 100x and 2500x were used for size statistics. Images without visible particulate matter were discarded. Labels were cropped out in preparation for image analysis.

In step three, the Trainable Weka Segmentation plugin for Fiji was used to segment images into "particle" and "background" classes.[15] I supplied Weka with example classifications on 10 images until there was subjective agreement between the automatically segmented images and the user-identified segments. When creating example classifications, I erred on the side of undercounting particles, because shape is of greater interest than particle count. The segmented images were converted into grayscale probability maps of particle locations. Figure 2 depicts the progression from original SEM micrograph to segmented image to probability map.

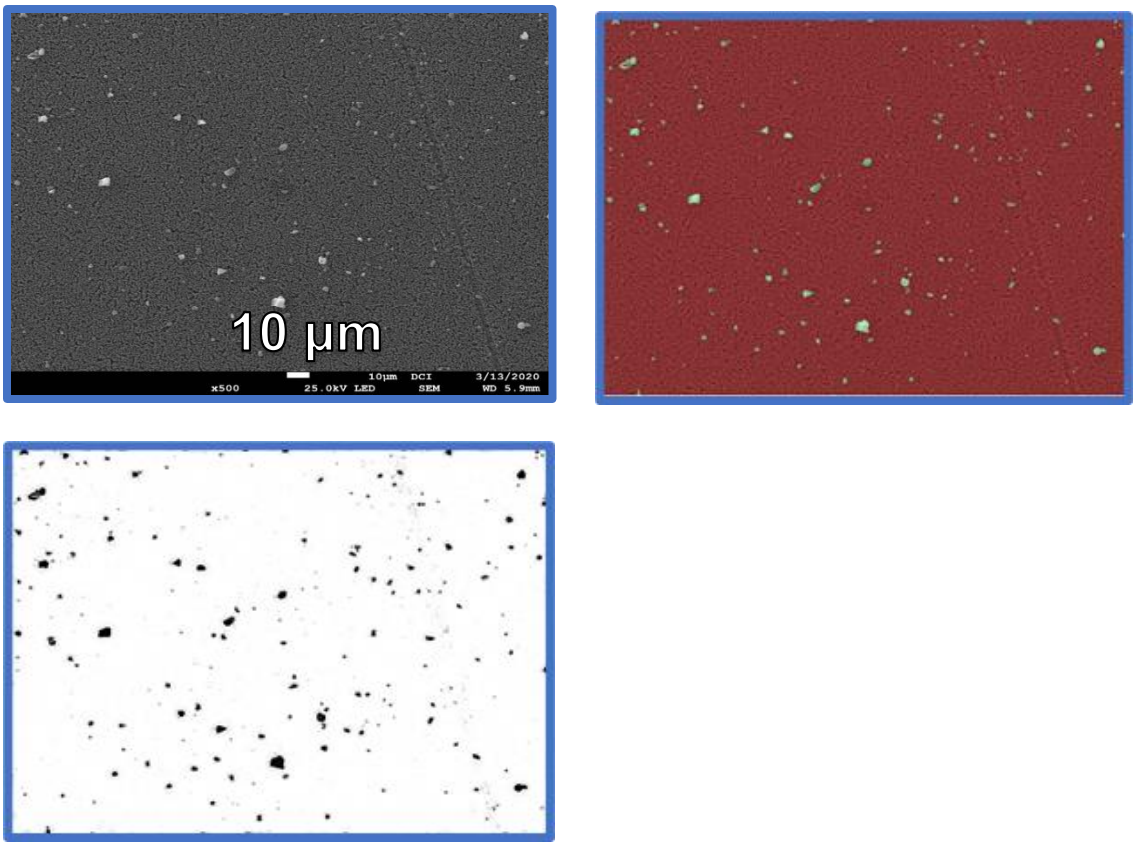

FIGURE 2. Original SEM Micrograph (top left), Weka Segmented Image (top right), Grayscale Probability Map (bottom left)

Each magnification required a unique segmentation scheme because of the changes in the appearance of the background membrane (*i.e.*, at lower magnifications the membrane appears uniform and at higher magnifications individual inhomogeneities are visible). Figure 3 compares the same background at 100x and 5000x magnifications, where it appears homogenous and heterogenous, respectively.

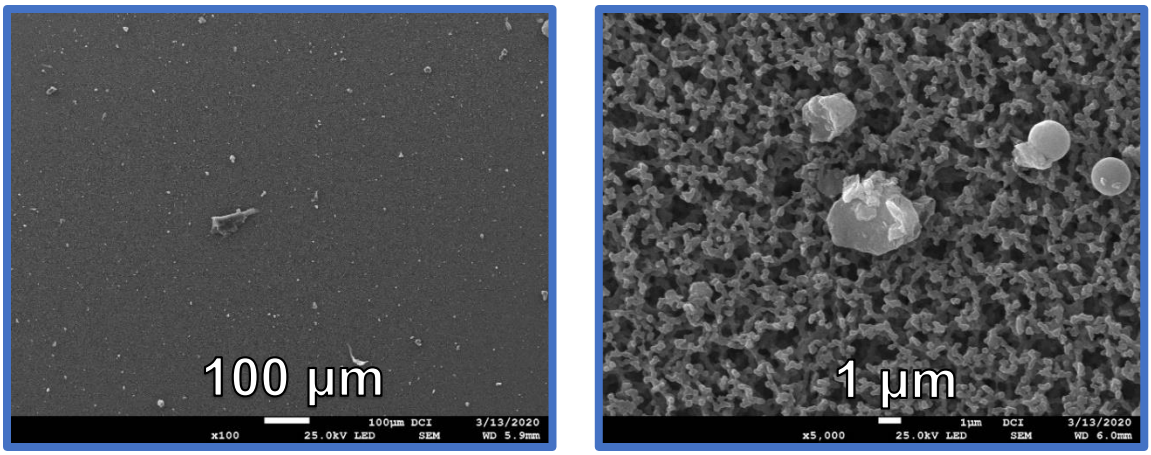

FIGURE 3. 100x SEM with Uniform Membrane Background (left), 5000x SEM with Visibly Inhomogeneous Membrane Background (right)

In step four, Tunwal *et al.*'s Image based Particle Shape Analysis Toolkit (IPSAT) was used to analyze the particles in each image for several pieces of size and shape data. IPSAT was originally developed for analysis of two-dimensional sedimentary grains in light micrographs for geology applications. However, it was directly applicable to the problem at hand and provided a means for gathering a much more robust collection of shape parameters for Arizona test dust than has been documented in the literature previously.

IPSAT was used to convert the grayscale probability maps into binary particle maps. Unique thresholds were selected for each magnification to produce a set of particles that subjectively agreed with user-identified particles. Each particle was then converted to an outline. Figure 4 depicts the progression from binary map to outline map to IPSAT-processed image. IPSAT calculated several size and shape parameters for each particle on the outline maps. The size and shape parameters are defined in Tables 1 and 2, respectively. The size and shape data were exported to Excel for analysis. In the future, improvements

could be made by correcting for particles on the edge of the field of view, overlapping particles, and particles that were erroneously segmented.

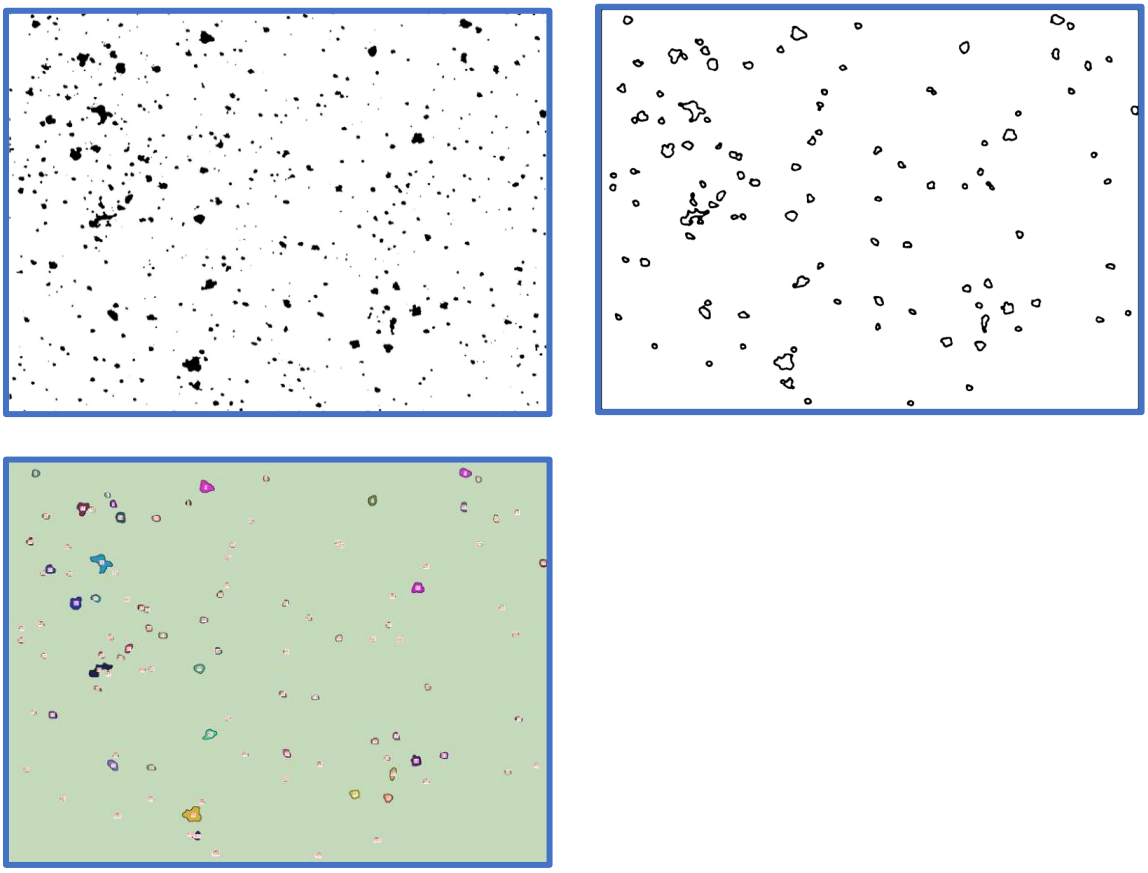

FIGURE 4. Binary Particle Map (top left), Outline Map (top right), IPSAT Image (bottom left)

TABLE 1. Definitions of IPSAT Size Parameters
(reproduced from Tunwal, *et al*.)[16]

Size Parameter	Formula	Description
S_c	D_c	Diameter of smallest circumscribing circle over a particle boundary
S_p	P/π	Perimeter, P, of particle boundary divided by pi
S_d	$\sqrt{4A/\pi}$	Diameter of a circle with an area, A, equivalent to that of the particle
S_a	L_{major}	Long axis of the best fit ellipse
S_b	L_{minor}	Short axis of the best fit ellipse
S_m	$\frac{2\sum_{i-1}^{n}(d_i)}{n}$	Twice the mean distance between the center and the particle boundary

TABLE 2. Definitions of IPSAT Shape Parameters
(reproduced from Tunwal, *et al*.)[16]

Size Parameter	Formula	Description
Aspect Ratio	S_a/S_b	Ratio of major axis to minor axis
Compactness	S_d/S_a	Ratio of S_d to S_a
Mod Ratio	$D_I/Feret$	Ratio of the diameter of the largest inscribed circle, D_I, to the Feret diameter
Solidity	A/A_{convex}	Ratio of particle area to convex area
Convexity	P_{convex}/P	Ratio of convex particle perimeter to perimeter
Rectangularity	A/A_{BR}	Ratio of particle area to area of bounding rectangle
Roundness	$R = \frac{1}{nr_{max}}\sum_{i=1}^{n} r_i$	r_{max}: radius of largest inscribed circle r_i: radius of curvature at corner i
Circularity	$C = \sqrt{D_I/D_C}$	D_I: diameter of largest inscribed circle D_C: diameter of smallest circumscribing circle
Irregularity	$I = A_U/A_E$	A_E: area of the best fit ellipse A_U: sum of area of best fit ellipse not overlapping with particle and area of particle not overlapping with best fit ellipse
Angularity	-	Average of the five largest differences in internal angle for all vertices along a particle outline.

In step five, a statistical analysis of the IPSAT data was performed. The data for each image were combined into a master JMP file with information on 3637 unique particles. Spurious data outside the possible range (*e.g.*, roundness greater than one) and data from small particles imaged at an insufficient zoom to reliably assess shape were excluded. According to Tunwal *et al.*, particles occupying fewer than 85 pixels can provide inconsistent results.[16] For safety, 200 pixels was the minimum size selected here. I derived equation 2 below to determine the minimum zoom for a corresponding particle area.

$$minimum\ zoom = 10^4 \cdot \left(\frac{200\ pixels}{particle\ area\ [um^2]}\right)^{1/2} \cdot \left(\frac{1\ um}{107\ pixels^{1/2}}\right) \qquad (2)$$

Next, a multivariate analysis was performed looking for correlations between shape parameters and the diameter of the smallest circumscribing circle over a particle boundary (S_c). This size parameter is of particular interest, because it is closest to what is generated by laser diffraction particle size analysis. This method of particle size analysis is the standard method used in the filtration field. Distribution data were collected for all other parameters.

Circularity is the only shape parameter that is even a moderate function of particle size (linear Pearson correlation coefficient, r = -0.48). Smaller particles tend to be more circular. This may partially be a result of the image processing, because the probability map approach could have the effect of softening particle borders which will more significantly impact the shape of smaller particles. The mean and median circularities are 0.77 and 0.80, respectively.

Dispersion in water appears to have introduced small (~1-2 μm), highly circular particles (Figure 5 left) that were not present in dry dispersions (Figure 5 right). The particles tend to charge more than their noncircular counterparts. It is not clear if these particles are a contaminant or the result of ISO fine components dissolving and subsequently drying. They have the effect of artificially increasing the apparent circularity of smaller particles.

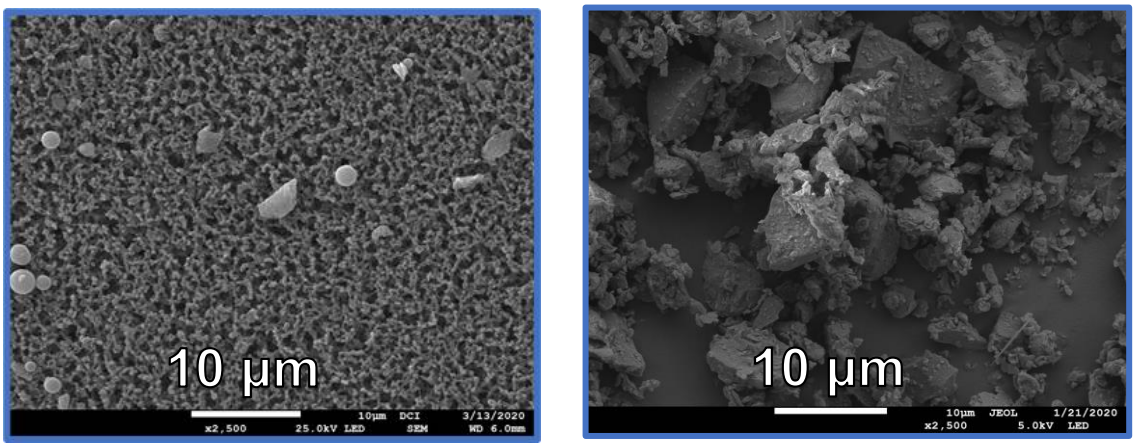

FIGURE 5. Highly Circular Particles (left), Comparable Dry Dispersion (right)

Typical ISO Fine Particle Shape Characteristics

Figures 6 and 7 depict the histogram distributions of the various shape parameters, which are summarized and explained here.

Irregularity

ISO Fine particles tend to be regular with mean and median irregularity values of ~0.2, which means the best fit ellipse and particle overlap approximately 80% of the time. By contrast, the spheres (circles in 2D) used in Donaldson models would have an irregularity of 0, meaning they are perfectly described by the best fit ellipse.

Aspect Ratio

ISO Fine particles have a typical aspect ratio of ~1.4. They are not excessively oblong. Spheres have an aspect ratio of 1.

Rectangularity

Rectangularity is another measure of irregularity. Values closer to one indicate higher regularity and a better ability to be described by a rectangle. 0.65 is a typical value for ISO Fine. Spheres have a rectangularity of 0.79 ($\pi/4$).

Compactness

A value of one indicates a circular particle whereas higher values are associated with more spread-out structures (*e.g.*, dendrites). ISO Fine tends to be compact with a typical value of 1.69. Spheres have a compactness of 1.

Solidity / Convexity

These are measures of particle outline convexity (as opposed to concavity). Values closer to one indicate a particle is primarily convex. ISO Fine dust is largely convex

with typical values of 0.93 and 0.84, respectively. Spheres have a solidity and convexity of 1.

Roundness

ISO Fine corners are moderately round (as opposed to perfectly round or sharp). The probability map approach may artificially inflate measures of roundness. A typical value is 0.58. Spheres have a roundness of 1.

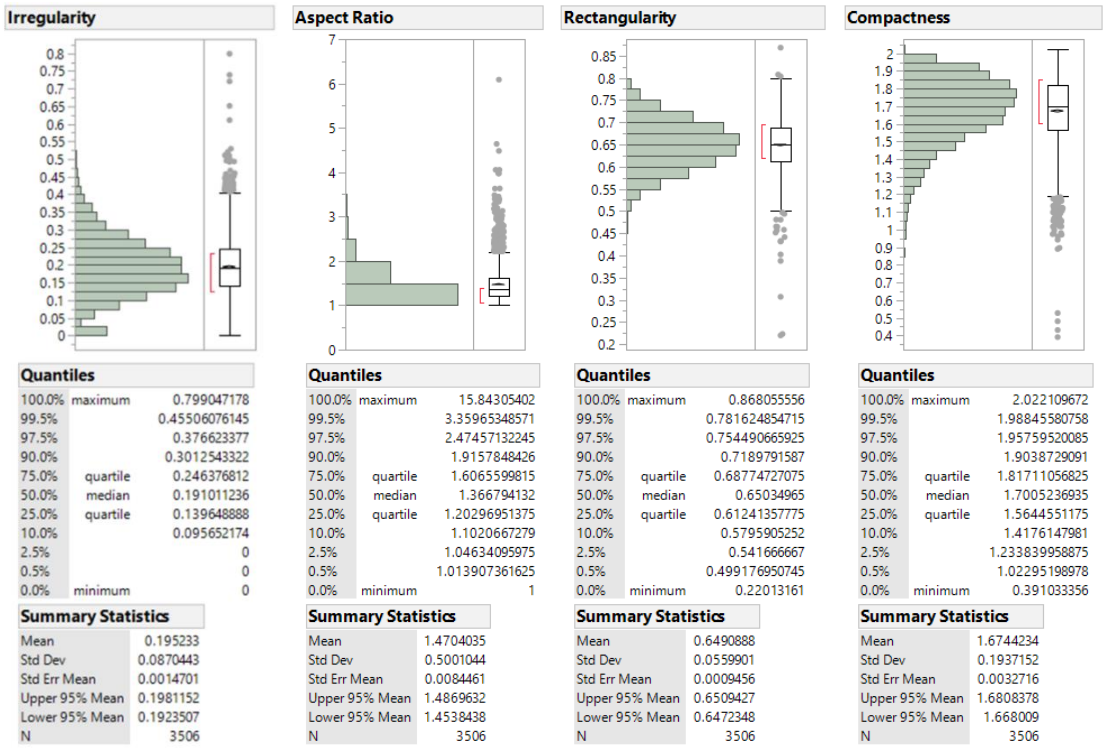

FIGURE 6. Distribution of Shape Parameters

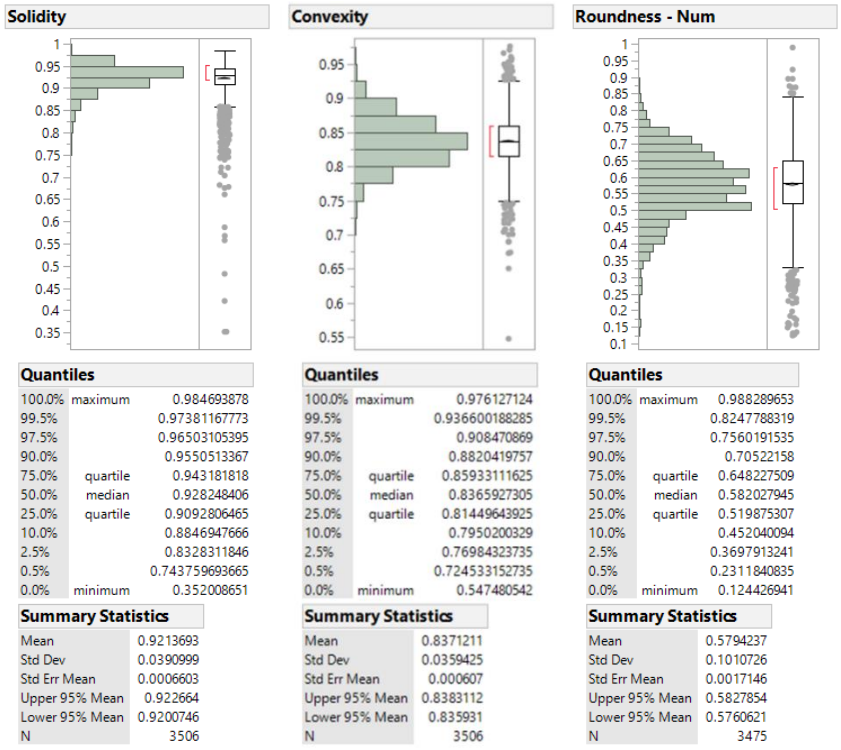

FIGURE 7. Distribution of Shape Parameters (continued)

Two general classes of particles were observed. The first is ISO Fine, which is crystalline, compact, regular, convex, and not easily described geometrically. The second is circular, which is nearly perfectly round and likely introduced through the dispersion process. An effort should be made to identify and understand the source of the circular particles. However, because they are not present in the undispersed ISO Fine dust, they will not be included in the 3D modeling effort. Other than the circular particles, there are not classes of simply defined geometric shapes that could be used for modeling (*e.g.*, squares, triangles).

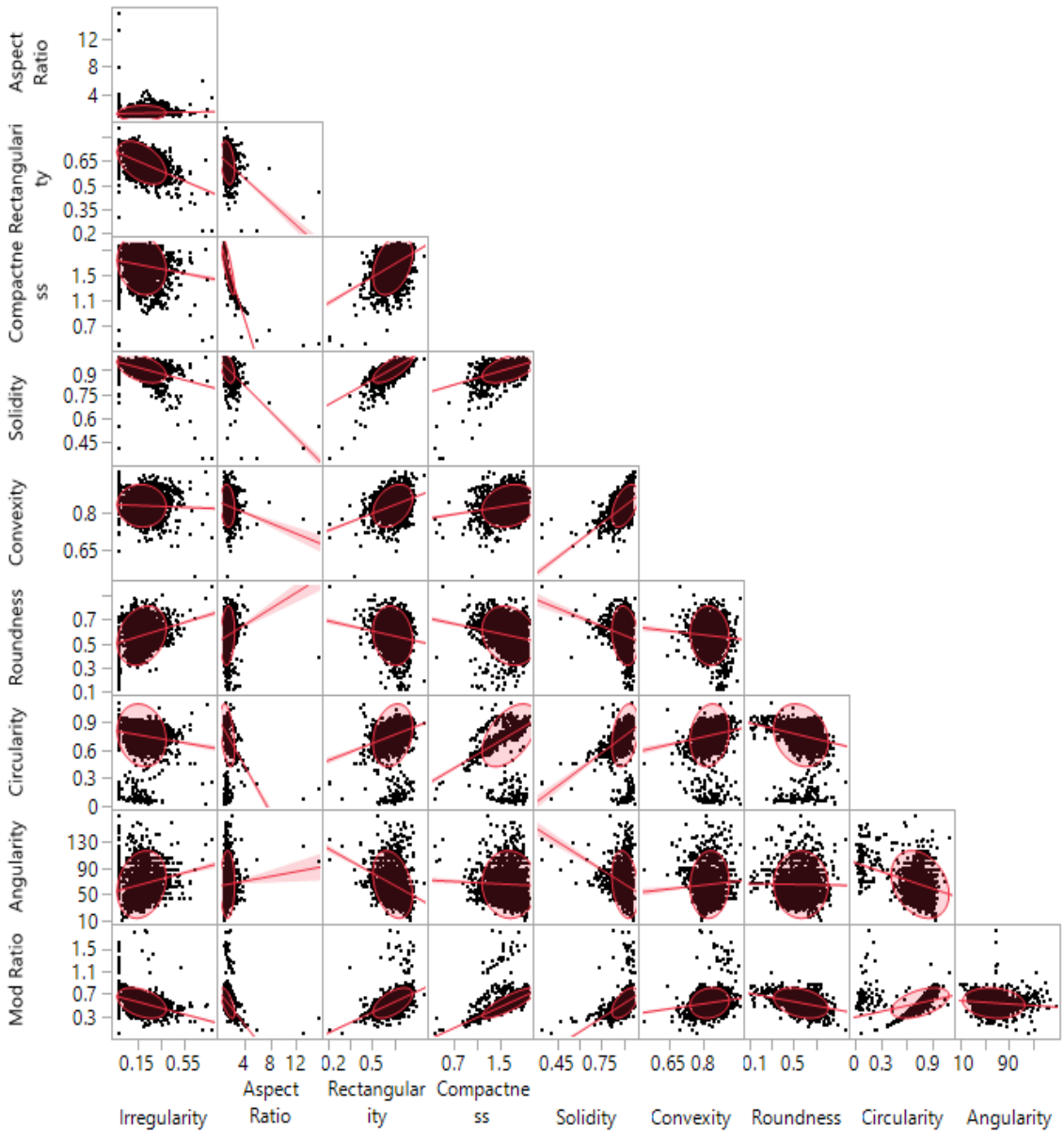

FIGURE 8. Scatterplot Matrix Depict Correlations Between Shape Parameters

TABLE 3. Summary of Two-Way Shape Parameter Correlations

	Irregularity	Aspect Ratio	Rectangularity	Compactness	Solidity	Convexity	Roundness - Num	Circularity - Num	Angularity - Num	Modratio - Num
Irregularity	1.0000	0.0637	-0.4834	-0.1587	-0.4364	-0.0458	0.2629	-0.1308	0.1945	-0.4004
Aspect Ratio	0.0637	1.0000	-0.3254	-0.8276	-0.5136	-0.1480	0.1255	-0.4340	0.0423	-0.6101
Rectangularity	-0.4834	-0.3254	1.0000	0.3960	0.7401	0.3627	-0.1615	0.2416	-0.3254	0.5759
Compactness	-0.1587	-0.8276	0.3960	1.0000	0.5337	0.2021	-0.1754	0.5068	-0.0417	0.7705
Solidity	-0.4364	-0.5136	0.7401	0.5337	1.0000	0.4994	-0.1768	0.3266	-0.2590	0.5509
Convexity	-0.0458	-0.1480	0.3627	0.2021	0.4994	1.0000	-0.0977	0.1357	0.0684	0.1761
Roundness - Num	0.2629	0.1255	-0.1615	-0.1754	-0.1768	-0.0977	1.0000	-0.1552	-0.0261	-0.3922
Circularity - Num	-0.1308	-0.4340	0.2416	0.5068	0.3266	0.1357	-0.1552	1.0000	-0.2930	0.4008
Angularity - Num	0.1945	0.0423	-0.3254	-0.0417	-0.2590	0.0684	-0.0261	-0.2930	1.0000	-0.1147
Modratio - Num	-0.4004	-0.6101	0.5759	0.7705	0.5509	0.1761	-0.3922	0.4008	-0.1147	1.0000

Figure 8 depicts all two-shape parameter combinations of scatterplots including best fit lines and 95% confidence ellipses. Table 3 summarizes the corresponding correlation coefficients. While size is a poor predicter of shape, multiple shape parameters do predict one another. The fact that many shape parameters correlate with one another derives from their related definitions. However, in a few cases shape parameters are correlated without obvious definitional overlaps.

Irregularity is moderately ($0.6>|r|\geq0.4$) negatively correlated with rectangularity, solidity, and mod ratio. It is weakly ($0.4>|r|\geq0.2$) positively correlated with roundness. The negative correlations can be rationalized by noting that irregularity and the other three parameters all quantify a particle's ability to be described by a regular geometric shape (either circle, ellipse, or rectangle). That is, if a particle is well-described by a rectangle, it will also be well-described by an ellipse (and vice versa). Best fit ellipses and rectangles overlap approximately 79% ($\pi/4$). The negative direction of the correlation is explained by the fact that irregularity is the inability to be described by a regular geometry, whereas the other three parameters are the corresponding ability. The weak positive correlation of irregularity and roundness does not follow from their definitions. One explanation is that ISO Fine is primarily crystalline silica, so the edges of a particle are expected to be sharp rather than round. Irregularity may indicate a deviation from the crystallinity and therefore also greater chance of roundness.

Aspect ratio is strongly ($|r|\geq0.6$) negatively correlated with compactness and mod ratio. It is moderately negatively correlated with solidity and circularity. It is weakly negatively

correlated with rectangularity. The strong negative correlation between aspect ratio and compactness is sensible given that, by definition, a convex particle (which these particles are) cannot be both compact and have a large aspect ratio. Similarly, high mod ratio particles are compact such that mod ratio must be negatively correlated with aspect ratio. To a lesser degree, but for similar reasons, a negative correlation follows from the definitions of solidity and circularity. The weak negative correlation between aspect ratio and rectangularity is less easily rationalized. After all, a shape can be perfectly rectangular but have a have a high aspect ratio if the difference between its major and minor sides is large. This would lead one to expect the parameters to be positively correlated. It can be seen from the scatterplot in Figure 8 that the direction of the correlation is driven by a small number of outlying particles with very large aspect ratios (>8) and low rectangularities (<0.5). Investigating these outliers individually shows that they are relatively concave, fibrous contaminants that are not representative of ISO Fine. Therefore, the small negative correlation is not likely to be meaningful.

Rectangularity is strongly positively correlated with solidity. It is moderately positively correlated with mod ratio. It is weakly positively correlated with convexity. It is weakly negatively correlated with angularity. The positive correlations derive from definitional overlap (especially with the restriction of high convexity). The weak negative correlation with angularity likely derives from the relationship with the lurking variable of circularity. Circularity and angularity are known to be negatively correlated for a variety of particle morphologies (beyond ISO Fine).[16] So the positive correlation between rectangularity and circularity drives the negative correlation between rectangularity and angularity.

Compactness is strongly positively correlated with mod ratio. It is moderately positively correlated with solidity and circularity. It is weakly positively correlated with convexity. The strong correlation with mod ratio arises from similarities in definition. Compactness is the ratio of a particle's equivalent area circle diameter to its major axis length. Mod ratio is a particle's inscribed circle diameter to its Feret diameter. Feret diameter (sometimes called caliper diameter) is often the same value as the major axis length or close to it. Further, as a particle becomes more compact its equivalent area circle diameter and inscribed circle diameter will converge. As a result, compactness and mod ratio vary closely together and in the same direction. Similar logic underlies the correlations with solidity and circularity. These correlations are weaker because of a lesser degree of definitional similarity. The lurking variable of solidity leads to the weak correlation with convexity.

Solidity is moderately positively correlated with convexity and mod ratio. It is weakly positively correlated with circularity. It is weakly negatively correlated with angularity. Definitional overlap explains the positive correlations. Tunwal informally describes angularity as the oppositive of circularity.[16] Since solidity varies positively with circularity, it is unsurprising that it varies negatively with angularity.

Roundness is weakly negatively correlated with mod ratio. This is explained by the fact that mod ratio varies directly with the diameter of the largest inscribed circle, but roundness varies as the inverse of that value. This drives the two values in opposite directions.

Circularity is moderately positively correlated with mod ratio. It is weakly negatively correlated with angularity. The positive correlation is explained by the fact that mod ratio varies directly with the diameter of the largest inscribed circle, but roundness varies as the square root of that value. This drives the two values in the same direction for diameters greater than one. Tunwal previously established that angularity and circularity are negatively correlated for a variety of particle geometries.[16]

In total, ISO Fine shape parameters and particle size appear not to be strongly correlated. This agrees with Fletcher, *et al.*'s findings for ISO Medium dust. Therefore, for 3D shape analysis it is not necessary to exhaustively model ISO Fine particles of all sizes. This dramatically reduces the number of particles that need to be fully described in three dimensions in order to create representative set of particles. Though at the same time, estimations of shape cannot be made simply based on characteristic size. The focus should be on small particles (< 10 μm), which are the majority of particles present in ISO Fine volume-based distributions.

CHAPTER 3: THREE-DIMENSIONAL STRUCTURE FROM MOTION

With two-dimensional characterization of ISO Fine complete, the next step is to expand to three dimensions. As discussed in the introduction, the motivation for this project is to improve the predictive power of filtration models and simulations via the creation of more realistic 3D dust particle representations. The available literature on Arizona test dust 3D morphology is even more limited than it is for 2D characterization. In one study, Woodward *et al*. used SEM and AFM to characterize the shape and roughness of Arizona Test dust.[17] They found dust to be well described as smooth, flat disks with a ratio of diameter to maximum height of about eight. Woodward *et al*. do not specify the variety (ISO Fine, ISO Coarse, etc.) of Arizona test dust they examined, but if the smoothness they detect holds for ISO Fine, it limits the amount of roughness resolution required to create a representative model. More importantly, the vast difference in particle height compared to particle diameter is not apparent in the thousands of Arizona test dust SEM images collected by Donaldson. This warrants further investigation.

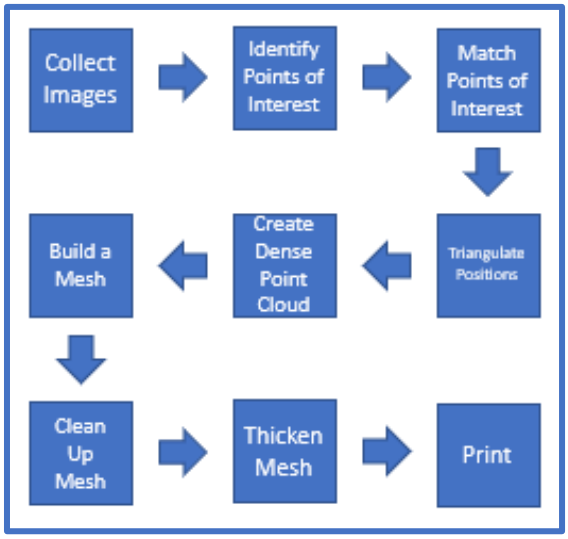

FIGURE 9. Scheme for Generation of 3D Dust Particle Models

Here, I follow a nine-step workflow (Figure 9) for the creation and printing of three-dimensional dust particle models. In step one, SEM micrographs of a single dust particle are collected at all combinations of seven tilts (φ = -5, 0, 5, 10, 15, 20, 25°) and six rotations (θ = 0, 60, 120, 180, 240, 300°) of the stage. A greater range of tilt angles is desirable, but this is the limit of the instrument. The effect of this limit is to reduce the fidelity of the z-direction resolution. An investigation into the minimum required number of rotation angles to produce a faithful 3D reconstruction of the particle was performed. I found that when images from two rotations (~180° apart) were used, the model dramatically overestimated the height of the particle compared to models generated from a greater number of rotations. When images from three rotations (~120° apart) were used, the model did not converge on a continuous surface. Images from four rotations (~90° apart), converged on a model that approximated those generated from a greater number of rotations. Figure 10 depicts models generated for various numbers of rotational angles. When subsequent particles were imaged with four-angle rotation scheme, they sometimes failed to converge. In practice, six angles produced the best results with the fewest number of images.

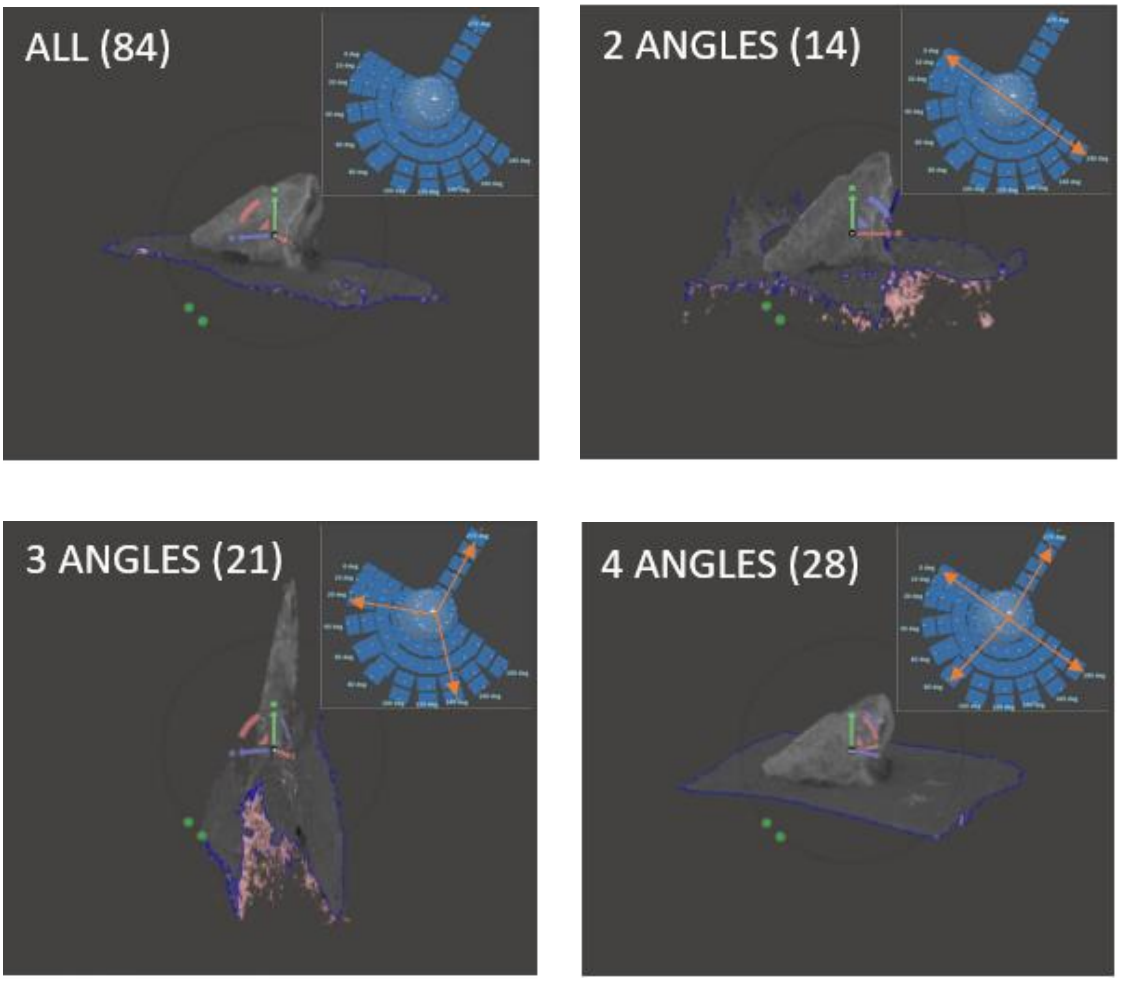

FIGURE 10. Models Generated from All, Two, Three, and Four Rotations

In step two, unique points of interest are identified in each image. Initial efforts attempted to follow built-in Matlab Structure from Motion capabilities.[18] Results failed to resolve without light camera calibration parameters (focal length, sensor size, *etc.*). Attempts to create SEM analogs of camera calibration parameters failed. Regard3D, an open source SfM, tool was able to identify points of interest from each image (Figure 11).

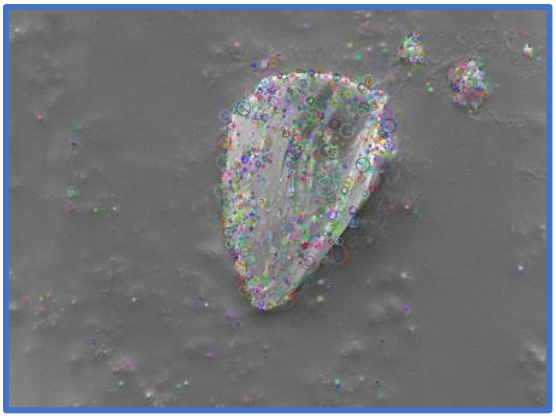

FIGURE 11. Points of Interest Identified with Regard3D

In step three, points of interest are tracked from image to image.[19] In Figure 12, the path of each point of interest is traced from its original location in the left image to its new location in the right image. Not all points of interest will be found in all images (or even more than one).

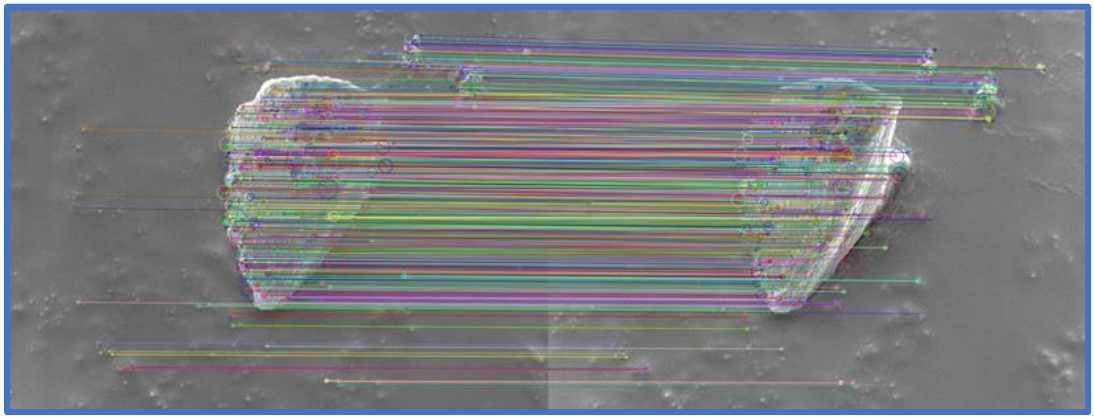

FIGURE 12. Motion of Points of Interest

In step four, the relative motion of points of interest from image to image is used to triangulate the position of those points in space. With Regard3D, this process failed (Figure 13, left) because of a lack of camera intrinsic properties similar to what occurred earlier

with Matlab's SfM capabilities. Again, attempts were made to "spoof" camera intrinsics by editing the SEM image exif metadata (Figure 13, right).[20] Unfortunately, a set of intrinsics that allowed the data to converge was not found.

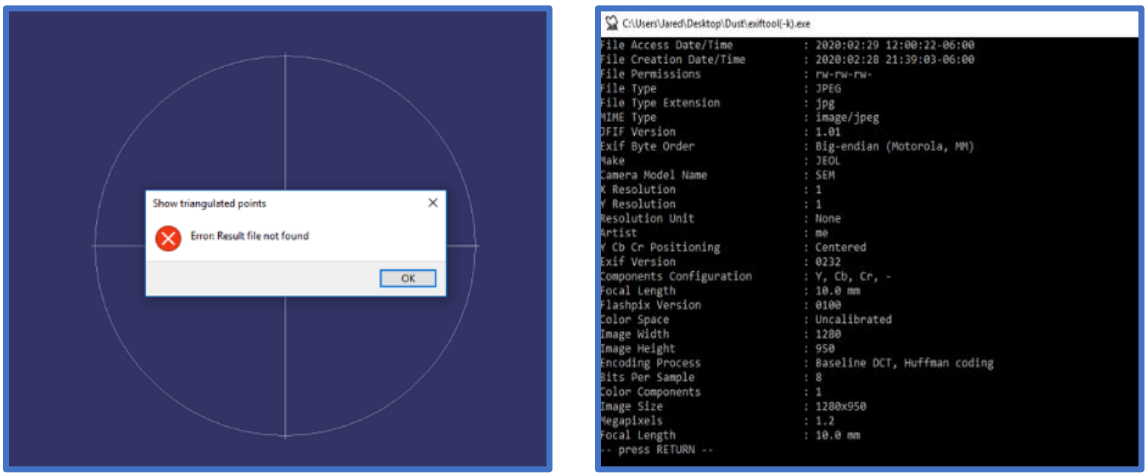

FIGURE 13. Regard3D Triangulation Error (left), ExifTool Metadata Editor (right)

Ball *et al.* demonstrated a successful SfM workflow for the creation of 3D models from SEM micrographs for educational purposes at the Natural History Museum in London.[21] The key advantage of their method over those previously described is that their software choice, Agisoft Photoscan, is able to triangulate relative positions in space without camera intrinsics. Therefore, I generally followed the scheme laid out by Ball *et al.* One key difference is that Ball *et al.* limited their investigation to 1000x magnification, whereas for this work the regime of interest was 10,000 to 20,000x. This precluded the use of automation, as the stage was incapable of sufficiently precise movements. Manual correction of stage positioning and focus were necessary. Another difference is the stage tilt capability. The NHM has an SEM with 90° tilt, but the Donaldson SEM is limited to 25°. It is possible that the lack of high tilt angle images leads to an overestimation of

particle height. This may explain why Woodward *et al.* found particles to be much more disk-like than this analysis did.

Agisoft Photoscan is used to complete steps two through four.[11] It successfully identifies relative spatial positions without absolute spatial data from camera intrinsics. The result is a 3D scatterplot of points of interest known as the key point cloud depicted in Figure 14.

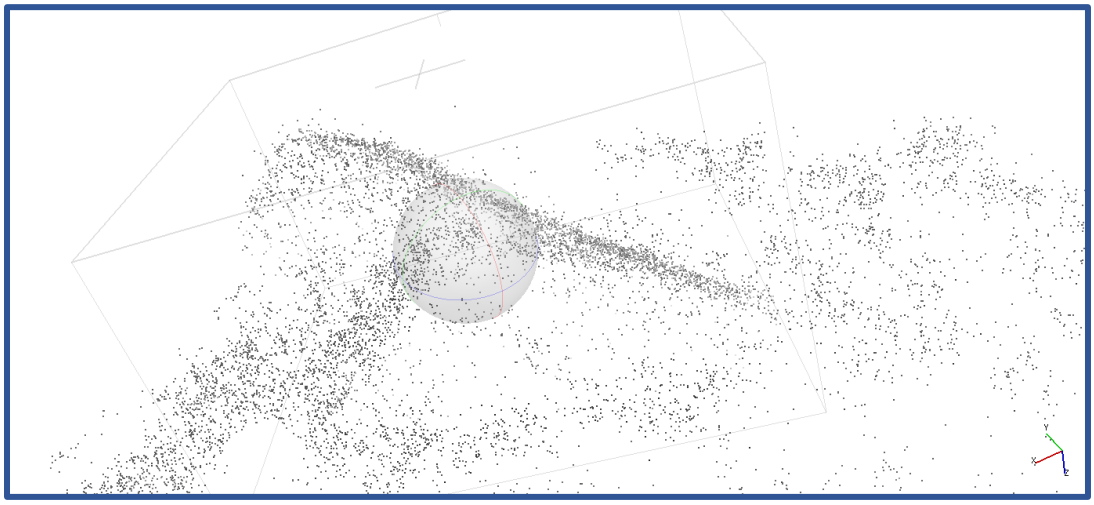

FIGURE 14. Key Point Cloud

In step five, additional points of interest are added to the key point cloud. These points of interest are present in fewer images (possibly just one) and confidence in their spatial position is lower. The resultant 3D scatterplot is known as a dense point cloud (Figure 15).

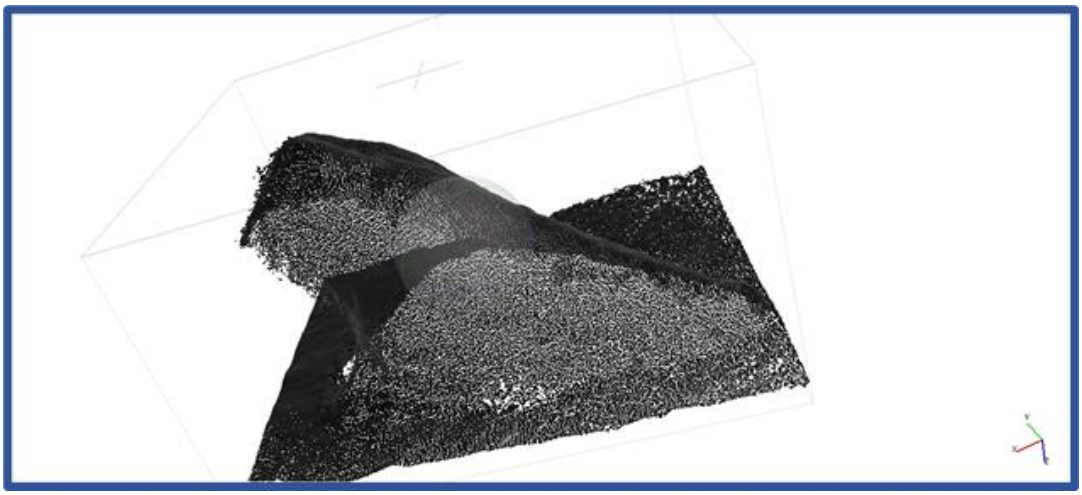

FIGURE 15. Dense Point Cloud

In step six, a mesh is created by plotting triangles between sets of three nearest neighbors in the dense point cloud. This mesh represents the outer perimeter of the dust particle (Figure 16).

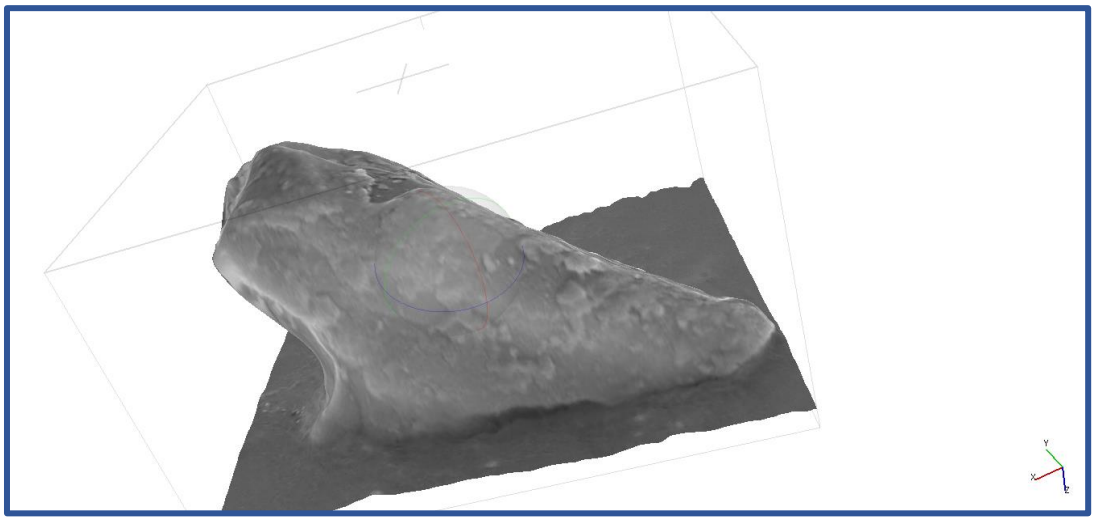

FIGURE 16. Mesh

In step seven, the mesh is exported to Meshmixer, software designed to prepare meshes for 3D printing.[22] The SEM stage is manually deleted from the mesh so that only the particle

remains. The Inspector tool is used to identify holes in the mesh above a specified threshold and then repair those holes (Figure 17, top left). The Make Solid tool softens sharp edges that are artifacts of the SfM process resulting in a lower resolution but higher fidelity model.

Following steps 1-7, the 3D particle model appears to be a faithful representation of the real particle with the exception of the face in contact with the SEM stage. This face is obscured from the SEM detector, so there is no data about this face. Without information, it appears to be a flat surface with sharp, discontinuous edges connecting it to the rest of the model (Figure 17, top right), which is clearly artificial when compared to the remainder of the particle. These sharp edges are likely to have a significant impact on any pressure drop experiments or simulations using reconstructions. Therefore, to mitigate the influences of these edges, with a high smoothing scale (~100%) and 2-4 constraint rings, the Deform→Smooth tool is used to round the edges and slightly inflate the obscured face (Figure 17, bottom left). This is consistent with the lack of sharp edges on the observable particle faces. At the same time, the surface remains smooth in the present reconstruction approach. In principle, surface roughness could be artificially added as discussed in the conclusion section.

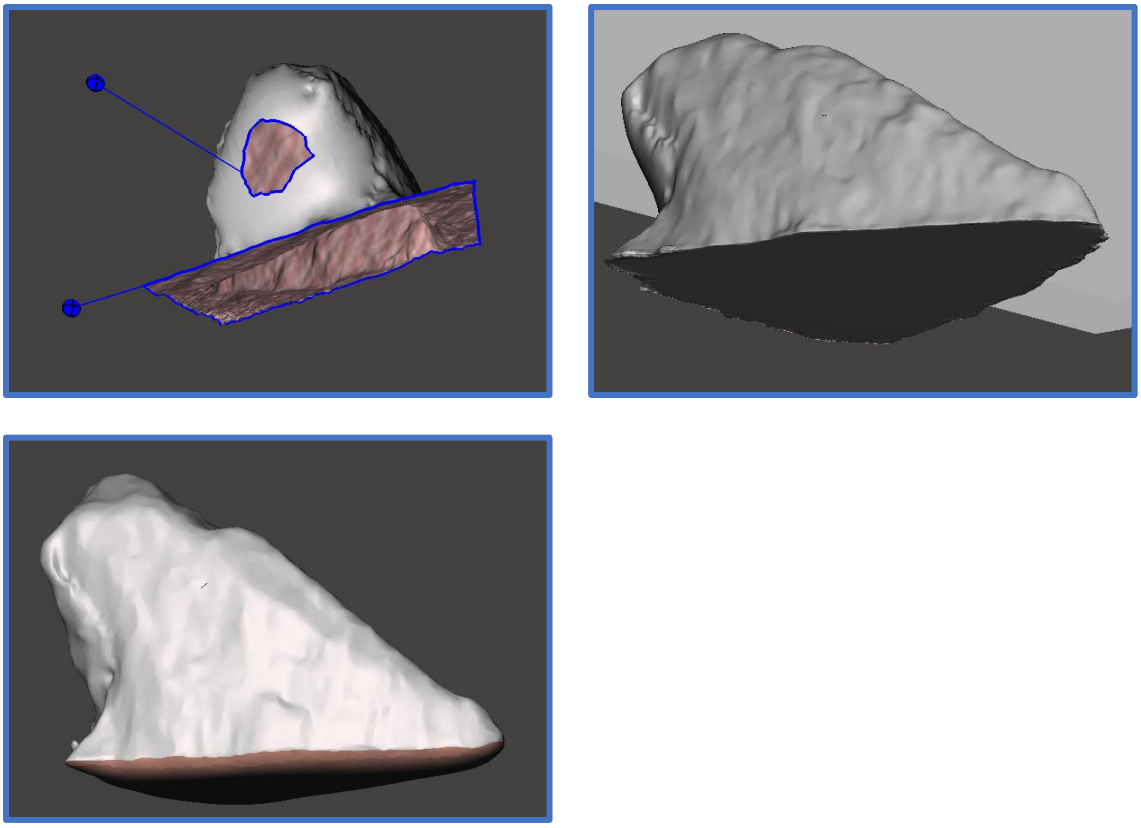

FIGURE 17. Imported Mesh (top left), Solid Mesh (top right), Rounded Mesh Bottom (bottom left)

In step eight, the mesh is given a nonzero thickness normal to the surface so that it is self-supporting. In step nine, the mesh is 3D printed, yielding a physical macroscale model of the individual dust grain. The first prototype particle is shown in Figure 18.

FIGURE 18. First Prototype 3D-Printed ISO Fine Particle Model

The process was repeated for four additional particles (Figure 19). As the models can be printed at a variety of sizes, through use of only several representative particles, a population of dust grains can be carefully defined and represented physically for experiments.

A comparison of these models as viewed from above with the earlier two-dimensional shape analysis indicates that these particles are typical of the overall distribution. At approximately four hours of labor per particle, this is a much more time intensive process than simply assuming the particles are spheres. This hence raises the question of whether the use of these more detailed shapes will lead to a meaningful difference in the outcome of modeling and simulation efforts (*i.e.,* is the additional effort to characterize dust and carry out reproduction worthwhile with regard to pressure drop modeling?). Modeling differential pressure across a filter as a packed bed using the Kozeny-Carman equation suggests it will be worthwhile. For example, the particle depicted in Figure 17 has a sphericity of 0.71 compared to 1 for a sphere, leading to 97% increase in the predicted

pressure drop for the same packing density. Even if this is an overestimation of the sphericity influence, it supports further experimentation with model dust reconstructions.

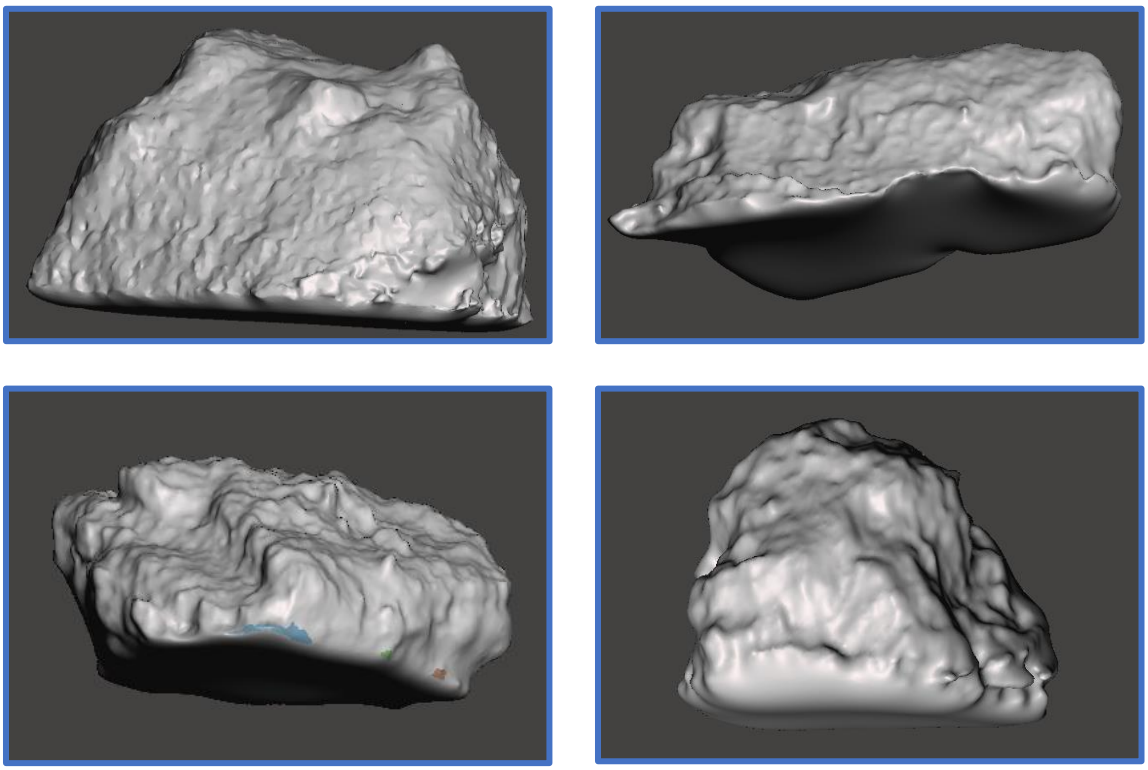

FIGURE 19. Additional Rounded Meshes

CHAPTER 4: PACKED BED EXPERIMENTS WITH 3D-PRINTED PARTICLES

Particle shape is expected to have a statistically and practically significant effect on resistance to flow (*i.e.*, pressure loss) across a loaded filter. This expectation is tested in the third phase by simulating the filter as a packed bed and measuring flow across the bed. In one condition the bed is packed with realistic particles 3D-printed at approximately 2000x their original size. In another condition, it is packed with an equal number of volume-equivalent spheres. Particle shape determines packing density, amount of exposed surface area, and both the length and sharpness of edges. Each of these factors will affect flow across a loaded filter. Increased packing density will increase differential pressure and decrease pulsability. Increased surface area will increase drag, impeding flow. Sharp edges may increase the ability of a particle to embed itself in the filter and will introduce flow discontinuities.

Real world experiments were chosen over computer simulations for two reasons. First, simulation of multiple structures with complex geometries is computationally intensive. This is partly why spheres are used in Donaldson's computer simulations. Second, it requires an understanding of the relevant, competing phenomena. These can be complicated and difficult to mathematically describe. For example, packing density of irregular structures is a standalone focus of computational research.[23, 24] Experiments are a simpler way to include these complexities without an explicit accounting. Furthermore, simulations require experimental validation. That is, the reconstruction effort developed

and applied here may eventually be used in simulations, but it is first necessary to compare those simulations to appropriate experiments.

Nonetheless, the experiments performed here are a preliminary effort to understand the effects of dust shape on pressure drop. A larger, robust system with a wide variety of particle distributions, which is beyond the scope of this work, would be needed to fully assess particle size distribution and shape effects on pressure drop in dust cakes. Furthermore, precise flow control is needed to match the Reynolds numbers for the scaled-up system to those of filters. Effort is made here to match Reynolds numbers by performing experiments with a viscous oil, as scaling up the particle size 2000x drastically increases the Reynolds number. However, the oil is not adequately viscous as the kinematic viscosity of gases is often as high or higher than liquids. A robust system would therefore require extremely low flowrates not achievable in the present system with measurable pressure drop present. A scaled-up packed bed was constructed as shown in the schematic and picture below (Figure 20, center and right, respectively). The packed bed consists of a 2' length of 4" diameter vertically oriented PVC tube, a grating for holding the packing material, and a ½" shutoff ball valve. Two different types of enlarged, 3D-printed packing media were selected: realistic dust particles and volume-equivalent spheres. Real ISO Fine particles have a log-normal size distribution. For practicality, only three sizes *(true chord length / printed chord length)* were used here: "small" (0.4 μm / 8 mm), "medium" (0.8 μm / 16 mm), and "large" (4 μm / 80 mm). These were printed in a ratio of ~160:80:1 based on laser diffraction particle size distribution data (Figure 20, left). Ultimately, the large

class of particles was abandoned due its disruption of packing without the presence of intermediate sizes.

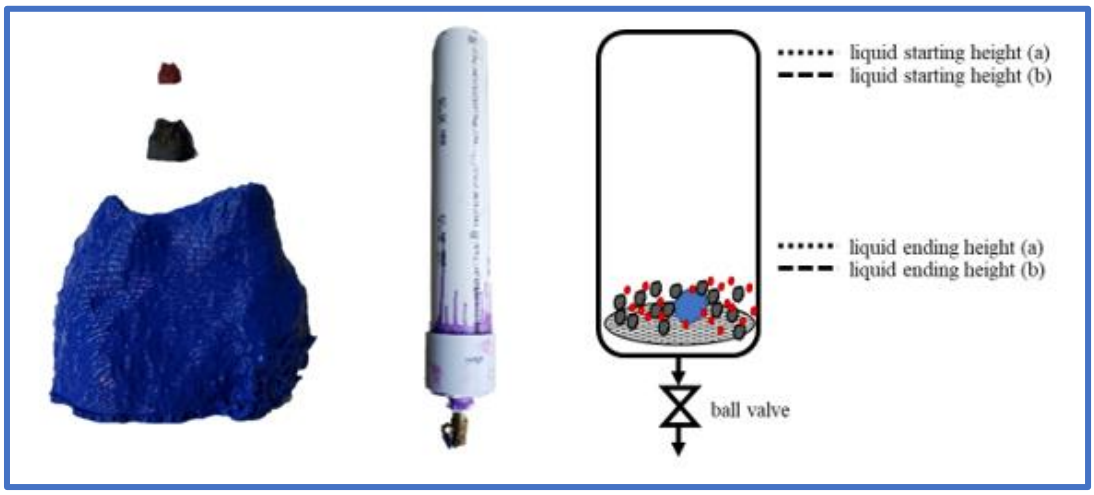

FIGURE 20. 3D-Printed Dust Particles (left), Packed Bed Photograph (center), Packed Bed Schematic (right)

A series of experiments was run to measure the effect of packing material geometry on resistance to flow. In each, the packed bed was filled with a liquid and the time to drain a set volume of liquid was recorded as a function of the packing material. Three packing conditions were considered: realistic dust particles, volume-equivalent spheres, and no packing material (control). The initial and final heights of the liquid were adjusted such that the starting and ending volumes of liquid were the same across all test conditions. Specifically, the volume of liquid between starting height (a) and starting height (b) was equal to the volume of the packing material. This ensured that pressure due to gravity on the liquid column was equivalent in all packing conditions. Additionally, ending heights were maintained above the packing material such that at all times the rate of emptying was affected by the resistance due to the packing material.

Each trial was repeated multiple times to average the effects of different particle packing configurations. That is, in each trial the particles were expected to pack together slightly differently, which could increase or decrease the resistance to flow depending on how tightly they packed. It was also done to minimize the effect of limited precision timing.

Water was selected as the liquid for the initial trials. The addition of realistic dust resulted in a 5% increase in drain time compared to the empty tube. This difference was found to be statistically significant with 99% confidence. However, volume-equivalent spheres were expected to have a drain time between that of the dust-packed bed and empty bed. At this level it would be difficult to distinguish between spheres and dust without a larger number of trials due to the limited ability to precisely measure such short time intervals. For this reason, the next series of trials was run with a higher viscosity liquid. This was expected to magnify the apparent difference in flow resistance.

TABLE 4. Packed Bed Drain Time When Filled with Water (left) and Canola Oil (right)

	Time (s)	
Trial	Empty	Dust-Packed
1	11.09	10.82
2	10.57	10.69
3	11.17	11.59
4	10.91	10.88
5	10.29	11.35
6	11.2	11.79
7	11.02	11.29
8	10.31	11.81
9	10.57	11.54
10	11.02	11.81
Average	10.82	11.36
St. Dev.	0.35	0.43
t-Test	6.36E-03	

	Time (s)		
Trial	Empty	Dust-Packed	Sphere-Packed
1	12.79	13.96	13.20
2	12.59	13.88	13.81
3	12.59	14.04	13.84
4	12.58	13.97	13.39
5	12.64	13.97	13.75
6	12.65	13.71	13.44
7	12.92	14.04	13.45
8	12.52	14.68	13.64
9	12.72	13.83	13.57
10	12.40	14.50	13.38
11	12.76	13.85	13.90
Average	12.65	14.04	13.58
St. Dev.	0.14	0.29	0.23
t-Test	Empty	6.87E-10	2.13E-09
	6.87E-10	Dust	5.79E-04
	2.13E-09	5.79E-04	Sphere

In the second set of trials, canola oil (~55 centipoise) was used as the test liquid. This had the desired result of magnifying the resistance to flow due to the packing material. The ratio of the dust cake pressure loss to the sphere pressure loss is proportional to the ratio of the corresponding emptying times minus the control emptying time.[25]

$$\frac{(time_{dust} - time_{control})}{(time_{sphere} - time_{control})} \propto \frac{Pressure_{dust}}{Pressure_{sphere}} \quad (3)$$

The pressure loss due to the dust is 49.6% greater than the pressure loss due to the volume-equivalent spheres. This is less than the 97% predicted difference from the Kozeny-Carmen equation. The prediction only accounts for the difference in sphericity, not other factors like packing efficiency. This may explain the deviations from the prediction. Results of the packed bed experiments are summarized in Table 4.

CHAPTER 5: CONCLUSION

"Garbage in, garbage out" is a common maxim in computer science. The output of a model is only as good as the quality of its inputs. This study was motivated by a desire to improve the predictive power of filtration modeling through the incorporation of realistic Arizona test dust particle morphologies. The main goal of the study was to demonstrate a robust, accessible method for measuring particle geometry in three dimensions and computationally reconstructing 3D particle geometries which are faithful to SEM images. A secondary goal was to test whether use of realistic particle shapes is of practical significance (*i.e.*, whether it leads to meaningfully different conclusions when compared to spherical particles).

The first step in this process is to describe particle morphology in two-dimensions. This study demonstrates a replicable workflow for doing so that uses image processing tools to assess diffuse particles imaged by SEM. The main conclusion from this portion of the study was that particle shape is largely independent of particle size for ISO fine test dust. Were this not the case, particles of a wide variety sizes would need to be modeled in 3D in order to create a representative subset. Instead, this suggests it is reasonable to model a small number of particles in 3D and then scale those models as needed.

The method demonstrated is readily applicable to other types of challenge particles whether they be surrogates (*e.g.*, PURAL alumina hydrate) or field samples (*e.g.*, agricultural dust).

The main limitation is the accuracy of the WEKA segmentation tool. It occasionally miscategorized the particle and background classes. By supplying a greater number of training images and having multiple operators prepare those images, one can expect the tool to more accurately match the result of human segmentation while doing so at rate that far outpaces humans. The IPSAT tool fails to account for particles on the edge of the field of view and overlapping particles. The first problem can be resolved by adding a step to the algorithm that disregards any particles that intersect with the image border. The second problem is more complicated. For geometrically regular particles, it has been studied and solutions have been proposed.[26] Those solutions are not applicable to geometrically irregular particles because they require a known, predictable particle shape. One practical solution is to further dilute the particle dispersion so that the probability of particles overlapping is reduced.

In the second step of this study, a readily implementable Structure from Motion method using commonly available analytical tools is demonstrated for the three-dimensional modeling of ISO Fine particles less than 10 microns in size. This approach avoids the pitfalls of common methods for assessing particle morphology: laser diffraction (requires *a priori* knowledge of particle shape), traditional SEM (limited to two dimensions), computed tomography (lacks sufficient resolution), and AFM (contact method, difficult to implement). As with the 2D method, the 3D method is applicable to a wide range of both regular and irregular challenge particles. If a challenge dust can be imaged by SEM, it likely can be modeled in 3D using the workflow demonstrated.

A key challenge with the approach described is the inability to automate the SEM imaging, which is the most time intensive part of the process. A solution to this would reduce operator time by about 75%. In the workflow, a particle of interest is centered, brought into focus, and then imaged from a variety of rotational and tilt angles. However, as the stage moves to new angles, the particle deviates from center. This is a result of the stage's inability to precisely rotate about the particle at high magnification. What the operator observes as a rotation about the particle is in fact a rotation of the stage about its center followed by a series of corrective translational motions. One approach to solve this is to make a series of small rotations (rather than one large one) and then employing a centering algorithm to bring the particle back into center. This should work provided 1) the particle does not fully exit the field of view and 2) it is sufficiently far away from other particles so that algorithm does not recenter on a new particle. Schorb, *et al.* developed a Realign Tool for TEM that has a similar functionality.[27]

Another limitation is the obscured particle face that is in contact with the stage and therefore inaccessible to the SEM probe. This is partially addressed here by rounding the edges and slightly inflating the face such that there are no artificial discontinuities. An improved approach would be to "wallpaper" surface topography from a visible face onto the obscured face. Further, statistics compiled on the 3D dimensional shape and roughness of ISO Fine could be used to procedurally generate representative particle models. Those are beyond the scope of the present work.

Woodward *et al*. found Arizona test dust particles to be much flatter using AFM than the present study did with SfM (height: diameter ~ 1:8 vs. 2:3). Accidentally embedding particles in the pinning medium is a risk with AFM, because it is a contact method. This would artificially decrease the height of particles. However, z-direction data for the SfM method was limited by the restricted tilt capability of the SEM used. This could have led the SfM algorithm to converge on an artificially taller structure. It is known that this is possible from the variation in the heights observed on structures produced from different numbers of rotational angles. The discrepancy with Woodward can be resolved by using an SEM with a greater tilt functionality to improve z-direction fidelity.

In the final step of the study, a series of pressure drop experiments using realistic dust particles and volume-equivalent spheres was performed. Those experiments show that realistic dust results in approximately 50% greater pressure loss than volume-equivalent spheres in a variety of combinations. In air filter applications an increase in pressure loss of this magnitude is of practical significance. By comparison, year-long filter development programs routinely target 10-25% differential pressure improvements.

The experiments performed here are intended as a proof-of-concept that demonstrates the value of using realistic dust morphologies rather than simple geometric surrogates. However, this idea can be extended to many other practical filtration applications. For example, these types of models can be used to simulate and better understand dust packing efficiency. This could be simulated computationally or tested practically using 3D printed models. In both cases a realistic particle morphology is needed. Dust packing efficiency

has important implications for pulsability, differential pressure, and filter life. A dust that packs more loosely will provide a lower pressure loss, pulse more efficiently, and last longer. Another application is the modeling of how particles orient in air streams. If spheres are used, the particles have no directionality. By contrast a particle with a non-unity aspect ratio, will often align is longest dimension in the direction of flow. This affects a particle's tendency to embed itself in filter media and how likely the particle is to be captured by a specific pore structure.

One recommendation for future experiments is to discretize the continuous particle size distribution with a greater number of particle sizes. Three is likely insufficient to fully reproduce the behavior of the continuum. This is a greater concern with real world experiments where there are practical limitations to how many particles can be reasonably printed.

A criticism of this approach is that the structures are too complicated to be simulated without impractically large computational power. Why not develop a transfer function between the realistic particle and spherical particle performance? A simple transfer function is unlikely to be found. The realistic morphology affects multiple factors (aerodynamics, packing, charge distribution, *etc.*). These would be difficult to fully address explicitly. This is expected to drive efforts toward empirical approaches. The structures found are easily down-scaled in resolution by reducing the number of triangles used in the mesh. One promising path is to use a series of down-scaled models to find the simplest structure that preserves the salient characteristics of the full 3D model.

REFERENCES

1. *Arizona Test Dust History*. Powder Technology Inc. (2020, June 15). https://www.powdertechnologyinc.com/test-dust-contaminants/test-dust-history/#.

2. International Organization for Standardization. (2016). Road vehicles — Test contaminants for filter evaluation (ISO Standard No. 12103-1).

3. Cho, G.-C., Dodds, J., & Santamarina, J. C. (2006). Particle shape effects on packing density, stiffness, and strength: Natural and crushed sands. *Journal of Geotechnical and Geoenvironmental Engineering*, *132*(5), 591–602. https://doi.org/10.1061/(asce)1090-0241(2006)132:5(591)

4. Saleem, M., Krammer, G., Khan, R. U., & Tahir, M. S. (2012). Influence of operating parameters on cake formation in pilot scale pulse-jet bag filter. Powder Technology, 224, 28–35. https://doi.org/10.1016/j.powtec.2012.02.016

5. Scott, D. M. (2019, December). *Interpreting Laser Diffraction Results for Non-Spherical Particles*. *Horiba Webinar Series*.

6. International Organization for Standardization. (2021). Nanotechnologies — Measurements of particle size and shape distributions by scanning electron microscopy (ISO Standard No. 19749:2021). https://www.iso.org/obp/ui/#iso:std:66235:en

7. Fletcher, R. A., & Bright, D. S. (2000). Shape Factors of ISO 12103-A3 (Medium Test Dust). *Filtration + Separation*, *37*(9), 48–56. https://doi.org/10.1016/s0015-1882(00)80200-1

8. du Plessis, A., Broeckhoven, C., Guelpa, A., & le Roux, S. G. (2017). Laboratory x-ray micro-computed tomography: A user guideline for biological samples. *GigaScience*, *6*(6). https://doi.org/10.1093/gigascience/gix027

9. Eaton, P., & Batziou, K. (2018). Artifacts and practical issues in atomic force microscopy. *Methods in Molecular Biology*, 3–28. https://doi.org/10.1007/978-1-4939-8894-5_1

10. *Structure from Motion*. Structure from Motion Overview - MATLAB & Simulink. (n.d.). https://www.mathworks.com/help/vision/ug/structure-from-motion.html.

11. *3D Model Reconstruction*. Agisoft Helpdesk Portal. (2020, October 8). https://agisoft.freshdesk.com/support/solutions/articles/31000152092.

12. Hixon, S. W., Lipo, C. P., Hunt, T. L., & Lee, C. (2017). Using structure from Motion mapping to record and Analyze details of the Colossal HATS (Pukao) of Monumental statues on Rapa Nui (Easter Island). *Advances in Archaeological Practice*, *6*(1), 42–57. https://doi.org/10.1017/aap.2017.28

13. Willis, M., Koenig, C., Black, S., & Castañeda, A. (2016). Archeological 3d mapping: The structure from motion revolution. *Index of Texas Archaeology Open Access Grey Literature from the Lone Star State*. https://doi.org/10.21112/ita.2016.1.110

14. Zhang, S. (2015). *Validity of Kozeny-Carman Equation in Constant-Pressure Cake Filtration* (thesis).

15. Arganda-Carreras, I., Kaynig, V., Rueden, C., Eliceiri, K. W., Schindelin, J., Cardona, A., & Sebastian Seung, H. (2017). Trainable weka segmentation: A machine learning tool for microscopy pixel classification. *Bioinformatics*, *33*(15), 2424–2426. https://doi.org/10.1093/bioinformatics/btx180

16. Tunwal, M., Mulchrone, K. F., & Meere, P. A. (2020). Image based Particle shape Analysis Toolbox (IPSAT). *Computers & Geosciences*, *135*, 104391. https://doi.org/10.1016/j.cageo.2019.104391

17. Woodward, X., Kostinski, A., China, S., Mazzoleni, C., & Cantrell, W. (2015). Characterization of Dust Particles' 3D Shape and Roughness with Nanometer Resolution. *Aerosol Science and Technology*, *49*(4), 229–238. https://doi.org/10.1080/02786826.2015.1017550

18. *Structure from motion from two views*. Structure From Motion From Two Views - MATLAB & Simulink. (n.d.). https://www.mathworks.com/help/vision/ug/structure-from-motion-from-two-views.html.

19. Hiestand, R. (n.d.). *Tutorial*. Regard3D. https://www.regard3d.org/index.php/documentation/tutorial.

20. Gronsbell, K. (2017, October 24). *Exiftool tutorial series*. AVP. https://www.weareavp.com/exiftool-tutorial-series/.

21. Ball, A. D., Job, P. A., & Walker, A. E. L. (2017). Sem-microphotogrammetry, a new take on an old method for generating high-resolution 3d models from sem images. *Journal of Microscopy*, *267*(2), 214–226. https://doi.org/10.1111/jmi.12560

22. *Meshmixer Manual*. Help. (n.d.). http://help.autodesk.com/view/MSHMXR/2019/ENU/?guid=GUID-9403A715-A108-4F7A-B500-3AF56AA2EEB0.

23. Majidi, B., Melo, J., Fafard, M., Ziegler, D., & Alamdari, H. (2015). Packing density of irregular shape particles: Dem simulations applied to anode-grade coke aggregates. *Advanced Powder Technology*, *26*(4), 1256–1262. https://doi.org/10.1016/j.apt.2015.06.008

24. Ma, Y., Chen, Z., Hu, W., & Wang, W. (2018). Packing irregular objects in 3d space via HYBRID Optimization. *Computer Graphics Forum*, *37*(5), 49–59. https://doi.org/10.1111/cgf.13490

25. Geankoplis, C. J., Hersel, A. A., & Lepek, D. H. (2018). *Transport processes and separation process principles*. Prentice Hall.

26. Zafari, S., Eerola, T., Sampo, J., Kalviainen, H., & Haario, H. (2015). Segmentation of overlapping elliptical objects in silhouette images. *IEEE Transactions on Image Processing*, *24*(12), 5942–5952. https://doi.org/10.1109/tip.2015.2492828

27. Schorb, M., Haberbosch, I., Hagen, W. J., Schwab, Y., & Mastronarde, D. N. (2019). Software tools for automated transmission electron microscopy. *Nature Methods*, *16*(6), 471–477. https://doi.org/10.1038/s41592-019-0396-9

APPENDIX

TABLE 5. Correlation Table of Size and Shape Parameters

	Irregularity	Aspect Ratio	Rectangularity	Compactness	Solidity	Convexity	SizeC	SizeP	SizeD	SizeA	SizeB	SizeM	Roundness - Num	Circularity - Num	Angularity - Num	Modratio - Num
Irregularity		0.0637	-0.4834	-0.1587	-0.4364	-0.0458		0.0766	0.0482	0.0719	0.0562		0.2543	-0.1324	0.1974	-0.4029
Aspect Ratio	0.0637		-0.3254	-0.8276	-0.5136	-0.148	0.1983	0.5475	0.3508	0.6191	0.1505	0.1063	0.1492	-0.4345	0.0427	-0.6108
Rectangularity	-0.4834	-0.3254		0.396	0.7401	0.3627	-0.0451	-0.2005	-0.1081	-0.2113	-0.0629		-0.1529	0.242	-0.3281	0.576
Compactness	-0.1587	-0.8276	0.396		0.5337	0.2021	-0.0498	-0.3236	-0.2728	-0.3508	-0.1507	-0.059	-0.1967	0.5073	-0.0418	0.7713
Solidity	-0.4364	-0.5136	0.7401	0.5337		0.4994	-0.1001	-0.4626	-0.3155	-0.476	-0.2486	-0.0817	-0.1815	0.3274	-0.2612	0.5516
Convexity	-0.0458	-0.148	0.3627	0.2021	0.4994			-0.2339	-0.227	-0.1925	-0.2194		-0.0764	0.1372	0.0661	0.1781
SizeC		0.1983	-0.0451	-0.0498	-0.1001			0.2517	0.1917	0.2555	0.1445	0.8417		-0.4778	0.1658	0.0447
SizeP	0.0766	0.5475	-0.2005	-0.3236	-0.4626	-0.2339	0.2517		0.9008	0.9855	0.8129	0.2162	0.0454	-0.1766	0.035	-0.2101
SizeD	0.0482	0.3508	-0.1081	-0.2728	-0.3155	-0.227	0.1917	0.9008		0.8256	0.9658	0.2103		-0.13		-0.1734
SizeA	0.0719	0.6191	-0.2113	-0.3508	-0.476	-0.1925	0.2555	0.9855	0.8256		0.7125	0.2078	0.0563	-0.1945	0.0426	-0.23
SizeB	0.0562	0.1505	-0.0629	-0.1507	-0.2486	-0.2194	0.1445	0.8129	0.9658	0.7125		0.1967		-0.063		-0.0831
SizeM		0.1063		-0.059	-0.0817		0.8417	0.2162	0.2103	0.2078	0.1967			-0.4741	0.1313	0.1559
Roundness - Num	0.2543	0.1492	-0.1529	-0.1967	-0.1815	-0.0764		0.0454		0.0563				-0.2088		-0.3376
Circularity - Num	-0.1324	-0.4345	0.242	0.5073	0.3274	0.1372	-0.4778	-0.1766	-0.13	-0.1945	-0.063	-0.4741	-0.2088		-0.2906	0.4013
Angularity - Num	0.1974	0.0427	-0.3281	-0.0418	-0.2612	0.0661	0.1658	0.035		0.0426		0.1313		-0.2906		-0.1264
Modratio - Num	-0.4029	-0.6108	0.576	0.7713	0.5516	0.1781	0.0447	-0.2101	-0.1734	-0.23	-0.0831	0.1559	-0.3376	0.4013	-0.1264	

	P > 0.05 or N/A
	Other r
	r < -0.75
	-0.75 < r < -0.50
	-0.50 < r < -0.02
	0.20 < r < 0.50
	0.50 < r < 0.75
	r > 0.75

TABLE 6. Probability Tables of Size and Shape Parameter Correlations

	Irregularity	Aspect Ratio	Rectangularity	Compactness	Solidity	Convexity	SizeC	SizeP	SizeD	SizeA	SizeB	SizeM	Roundness - Num	Circularity - Num	Angularity - Num	Modratio - Num
Irregularity	<.0001	0.0002	<.0001	<.0001	<.0001	0.0072	0.3203	<.0001	0.0046	<.0001	0.001	0.9021	<.0001	<.0001	<.0001	<.0001
Aspect Ratio	0.0002	<.0001	<.0001	<.0001	<.0001	<.0001	<.0001	<.0001	<.0001	<.0001	<.0001	<.0001	<.0001	<.0001	0.012	<.0001
Rectangularity	<.0001	<.0001	<.0001	<.0001	<.0001	<.0001	0.008	<.0001	<.0001	<.0001	0.0002	0.1455	<.0001	<.0001	<.0001	<.0001
Compactness	<.0001	<.0001	<.0001	<.0001	<.0001	<.0001	0.0034	<.0001	<.0001	<.0001	<.0001	0.0005	<.0001	<.0001	0.0141	<.0001
Solidity	<.0001	<.0001	<.0001	<.0001	<.0001	<.0001	<.0001	<.0001	<.0001	<.0001	<.0001	<.0001	<.0001	<.0001	<.0001	<.0001
Convexity	0.0072	<.0001	<.0001	<.0001	<.0001	<.0001	0.1349	<.0001	<.0001	<.0001	<.0001	0.9188	<.0001	<.0001	0.0001	<.0001
SizeC	0.3203	<.0001	0.008	0.0034	<.0001	0.1349	<.0001	<.0001	<.0001	<.0001	<.0001	<.0001	0.0728	<.0001	<.0001	0.0086
SizeP	<.0001	<.0001	<.0001	<.0001	<.0001	<.0001	<.0001	<.0001	<.0001	<.0001	<.0001	<.0001	0.0077	<.0001	0.0399	<.0001
SizeD	0.0046	<.0001	<.0001	<.0001	<.0001	<.0001	<.0001	<.0001	<.0001	<.0001	<.0001	<.0001	0.0921	<.0001	0.266	<.0001
SizeA	<.0001	<.0001	<.0001	<.0001	<.0001	<.0001	<.0001	<.0001	<.0001	<.0001	<.0001	<.0001	0.0009	<.0001	0.0123	<.0001
SizeB	0.001	<.0001	0.0002	<.0001	<.0001	<.0001	<.0001	<.0001	<.0001	<.0001	<.0001	<.0001	0.5785	0.0002	0.1023	<.0001
SizeM	0.9021	<.0001	0.1455	0.0005	<.0001	0.9188	<.0001	<.0001	<.0001	<.0001	<.0001	<.0001	0.9138	<.0001	<.0001	<.0001
Roundness - Num	<.0001	<.0001	<.0001	<.0001	<.0001	<.0001	0.0728	0.0077	0.0921	0.0009	0.5785	0.9138	<.0001	<.0001	0.3852	<.0001
Circularity - Num	<.0001	<.0001	<.0001	<.0001	<.0001	<.0001	<.0001	<.0001	<.0001	<.0001	0.0002	<.0001	<.0001	<.0001	<.0001	<.0001
Angularity - Num	<.0001	0.012	<.0001	0.0141	<.0001	0.0001	<.0001	0.0399	0.266	0.0123	0.1023	<.0001	0.3852	<.0001	<.0001	<.0001
Modratio - Num	<.0001	<.0001	<.0001	<.0001	<.0001	<.0001	0.0086	<.0001	<.0001	<.0001	<.0001	<.0001	<.0001	<.0001	<.0001	<.0001